

Detection of spike-like structures near the front of type-II bursts

S. Armatas¹ C. Bouratzis¹ A. Hillaris¹ C.E. Alissandrakis² P. Preka-Papadema¹ X. Moussas¹ E. Mitsakou¹ P. Tsitsipis³
and A. Kontogeorgos³

¹ Department of Physics, University of Athens, 15783 Athens, Greece
e-mail: kbouratz@phys.uoa.gr

² Department of Physics, University of Ioannina, 45110 Ioannina, Greece

³ Department of Electronics, Technological Educational Institute of Sterea Hellas, 35100 Lamia, Greece

Received; accepted

ABSTRACT

Aims. We examine high time resolution dynamic spectra for fine structures in type II solar radio bursts

Methods. We used data obtained with the (SAO) receiver of the Artemis-JLS (ARTEMIS-IV) solar radio spectrograph in the 450–270 MHz range at 10 ms cadence and identified more than 600 short, narrowband features. Their characteristics, such as instantaneous relative bandwidth and total duration were measured and compared with those of spikes embedded in type IV emissions.

Results. Type II associated spikes occur mostly in chains inside or close to the slowly drifting type II emission. These spikes coexist with herringbone and pulsating structures. Their average duration is 96 ms and their average relative bandwidth 1.7%. These properties are not different from those of type IV embedded spikes. It is therefore possible that they are signatures of small-scale reconnection along the type II shock front.

Key words. Sun: corona – Sun: radio radiation – Sun: activity – Sun: Radiation mechanisms: non-thermal

1. Introduction

Solar type II radio bursts are thought to be signatures of either shocks driven by coronal mass ejections (CME) or flare blast shock waves (Vršnak & Cliver 2008; Pick & Vilmer 2008). The radio emission is the result of energetic electrons accelerated by the shock. On the dynamic spectra they appear as slowly drifting bands, dubbed backbone, from high to low frequencies (Roberts 1959; Krueger 1979). The type II radio bursts often exhibit a characteristic fundamental-harmonic (F-H) structure (Maxwell & Thompson 1962) and sometimes show a split in two lanes by a small frequency offset of $\approx f/8$ – $f/4$ (Smerd et al. 1975; Vršnak et al. 2004).

Type II bursts exhibit fine structure. A common feature is the so-called herringbone structure, which is attributed to shock-accelerated electrons producing narrow bandwidth, type III-like groups, originating at the backbone and drifting toward higher and lower frequencies (Roberts 1959; Cairns & Robinson 1987). Slow drift fiber-like structures were reported by Chernov (1997) and Chernov et al. (2007) and interpreted as whistler wave packets upstream of the shock front. Narrowband drifting fibers, thought to be the result of type II emission refracted on inhomogeneous structures of the CME preceding the shock, have also been reported by Afanasiev (2009).

Spike bursts, which are abundant in type IV emissions (e.g., Bouratzis et al. 2016), are conspicuously absent from the type II fine structure, apart from one report (Chernov 2016) of spike-like structures in a single decametric event. The spike bursts have very short duration (~ 100 ms in the metric frequency range) and bandwidth (~ 1 – 2%) and are thought to be the signature of small-scale electron acceleration events through magnetic reconnection (Nindos & Aurass 2007).

We report the detection of narrowband spike-like structures, which are shorter than 100 ms and embedded in type II burst harmonic emission, in observations obtained with the high time resolution (10 ms) Artemis-JLS acousto-optic spectrograph (SAO) receiver in the 450–270 MHz range. In section 2 we describe our observations and data reduction followed by an overview of the events selected for study (section 3) and the presentation of their fine structure (section 4). Results are summarized and discussed in section 5.

2. Observations and data reduction

The Artemis-JLS (ARTEMIS-IV) solar radio spectrograph has been operating at Thermopylae since 1996 (Caroubalos et al. 2001; Kontogeorgos et al. 2006). The observations cover the frequency range from 20 to 650 MHz. The spectrograph has a 7 m moving parabola fed by a log-periodic antenna for the 100–650 MHz range and a stationary inverted V fat dipole antenna for the 20–100 MHz range. Two receivers operate in parallel: a sweep frequency analyzer (ASG) covering the 650–20 MHz range in 630 channels with a cadence of ten samples/sec and a low-noise, high sensitivity multi-channel acousto-optical analyzer (SAO), which covers the 270–450 MHz range in 128 channels with a time resolution of 10 ms.

Information about the corresponding flares such as location, class, and importance were obtained from the National Oceanic and Atmospheric Administration (NOAA) catalog. Information about associated CMEs was acquired from the Large Angle and Spectrometric Coronagraph (LASCO) on board the Solar and Heliospheric Observatory (SoHO) mission (Brueckner et al. 1995) and the CME catalog (Gopalswamy et al. 2009). From a large number of type II bursts observed with Artemis-JLS/ASG in the 1998–2013 period we selected four events that were well

Send offprint requests to: C. Bouratzis

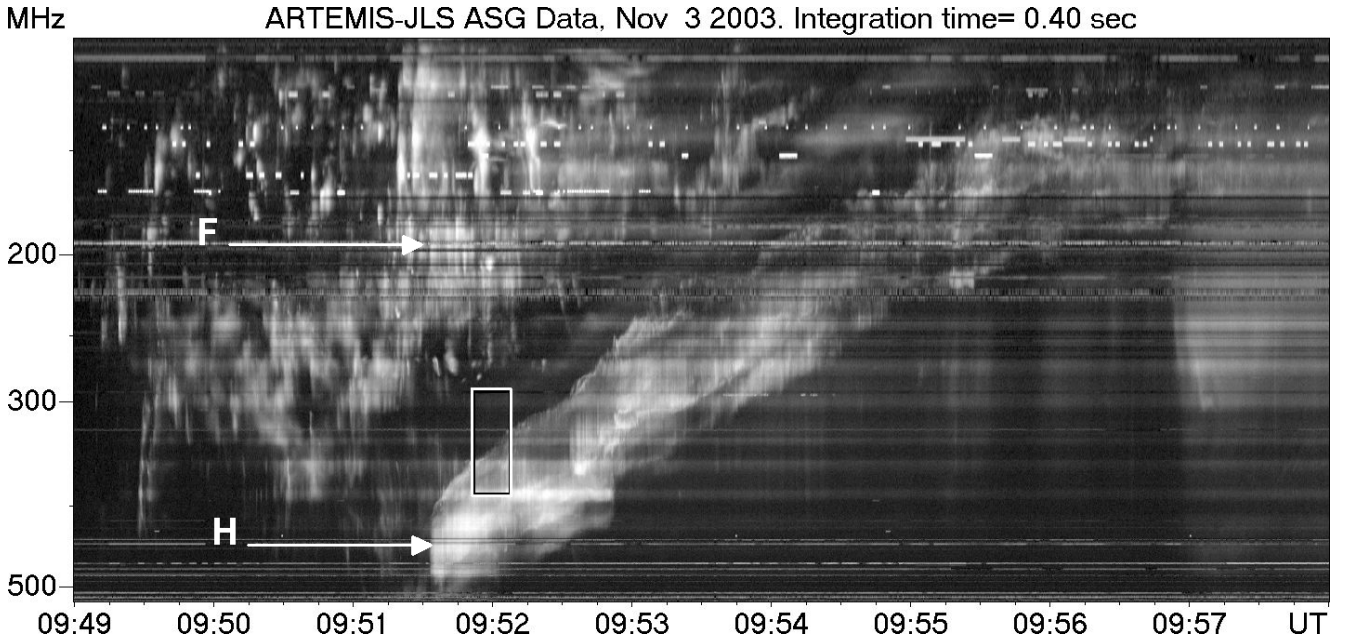


Fig. 1. Dynamic spectrum of the complex first event (SOL2003-11-03T09:43:20), observed with the Artemis-JLS/ASG receiver. The box indicates the segment discussed in Sect. 4 and the arrows the fundamental (F) and harmonic (H) lanes.

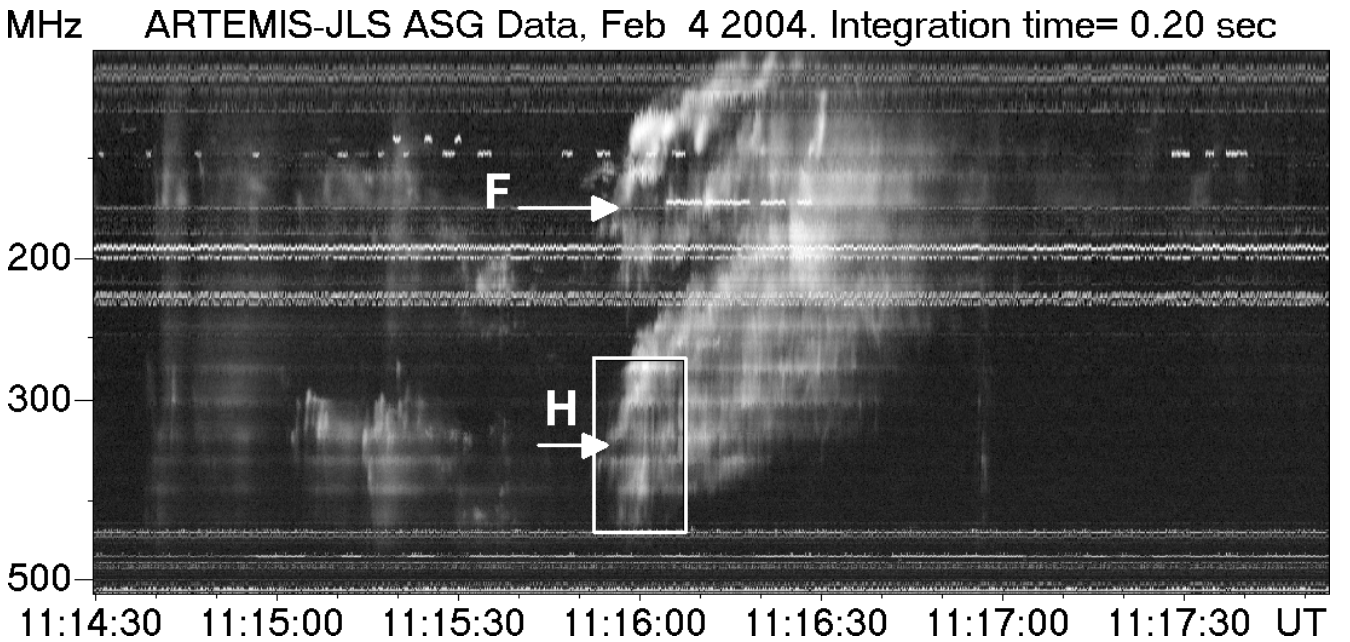


Fig. 2. Same as Fig. 1 for the second event, SOL2004-02-04T11:12:00.

covered by SAO receiver at frequencies above 270 MHz. All flares associated with these events occurred at longitudes $\geq 50^\circ$.

3. Overview of the selected events

The first event (2003 November 3, SOL2003-11-03T09:43:20) was related to a GOES X3.9 class flare at $08^\circ\text{N } 77^\circ\text{W}$ in AR 10488 near the west limb. The flare started at 09:43 UT and reached peak intensity at 09:55 UT. A CME was first detected at 10:06 UT with a backward-extrapolated lift-off at 09:53 UT.

Fig. 1 shows an expanded view of event observed with the ASG receiver of Artemis-JLS. The dynamic spectrum

shows the type II burst, which has a relative frequency drift $df/fdt=0.005\text{ s}^{-1}$, and associated type III and IV radio bursts. During the rise phase of the flare, a group of type III bursts overlap the fundamental emission of the type II burst in the 270 to 30 MHz range. The type II harmonic starts at 09:51:30 UT and 520 MHz, mostly within the Artemis-JLS/SAO frequency range.

The second event (2004 February 04, SOL2004-02-04T11:12:00) was associated with a C9.9 GOES flare, which occurred at 11:12 UT, $07^\circ\text{S } 49^\circ\text{W}$ (AR 10547), and a CME, which was observed by LASCO at 11:54 UT (backward-extrapolated lift-off time 11:19:28 UT). Fig. 2 presents an overview of the type II F-H burst with a relative drift rate of 3.8 s^{-1} and the asso-

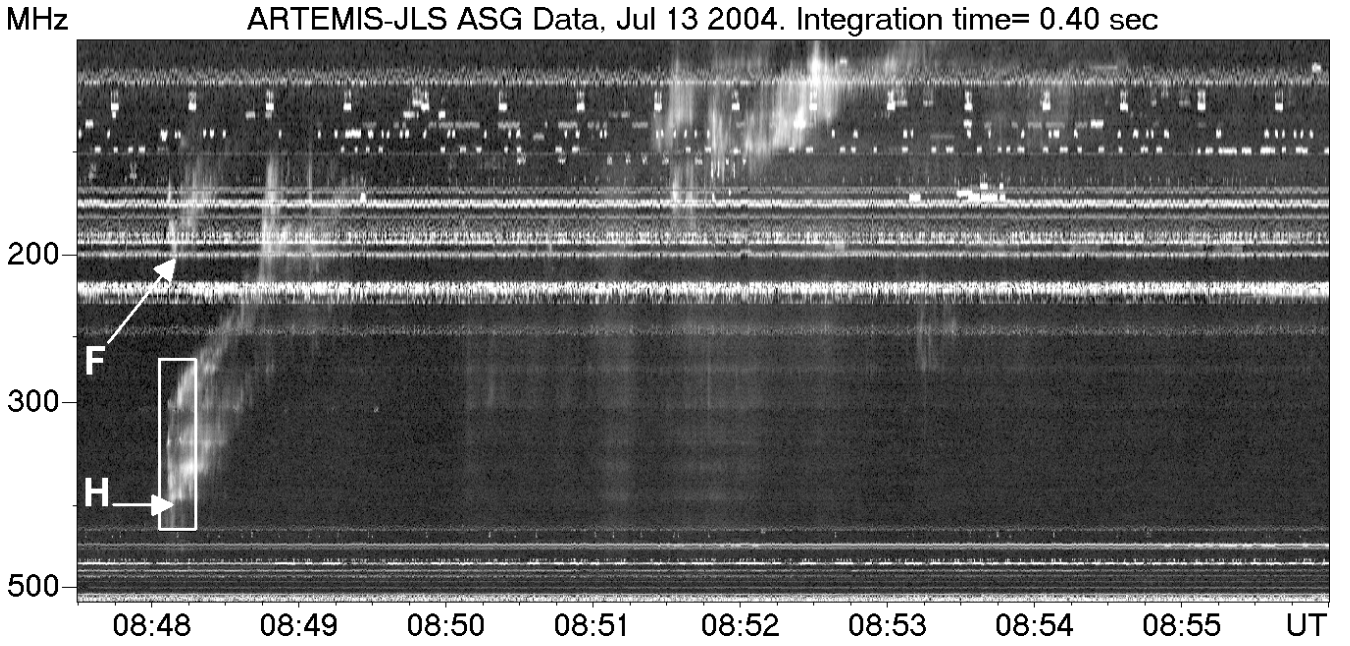


Fig. 3. Same as Fig. 1, for the third event, SOL2004-07-13T08:40:00.

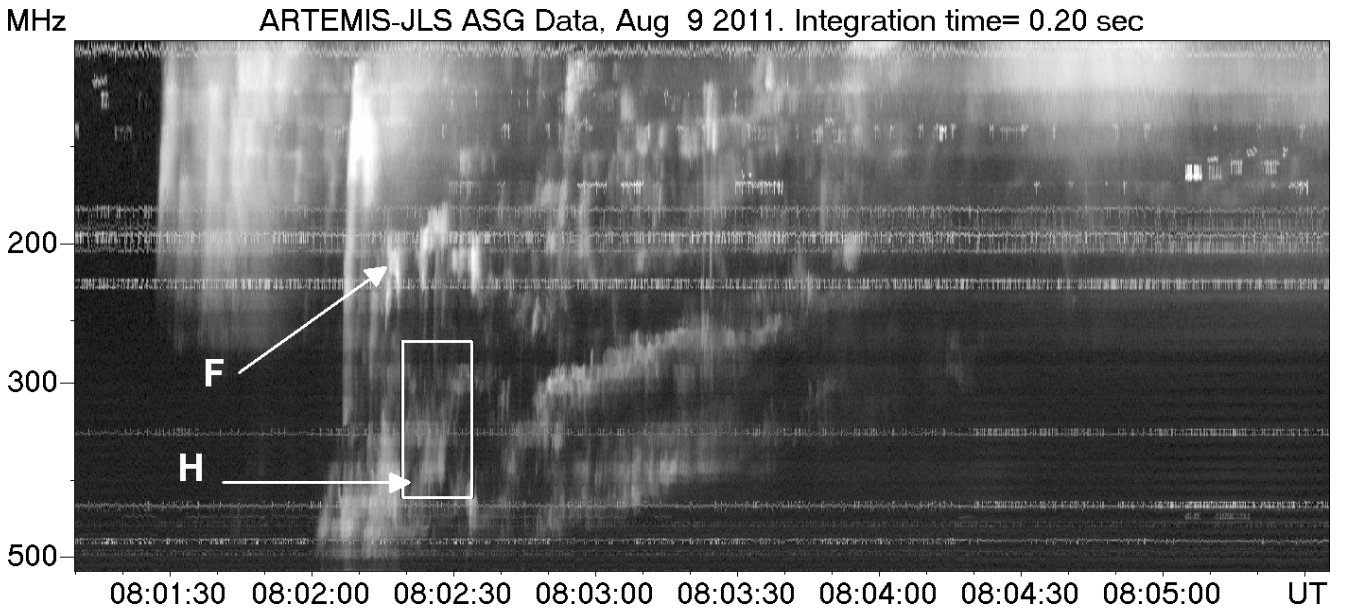


Fig. 4. Same as Fig. 1 for the fourth event, SOL2011-08-09T07:48:00.

ciated activity which includes the precursor of the type II burst (Klassen et al. 2003).

The third event (2004 July 13, SOL2004-07-13T08:40:00) was related to a GOES M5.4 flare at 12° N52 $^{\circ}$ W (AR 10646) and a halo CME. The flare started at 08:40 UT and reached its peak intensity at 08:48 UT, while the CME lift-off was at 08:46 UT. Spectral radio observations from ARTEMIS-JLS/ASG in the 20–500 MHz range are presented in Fig.3. A small group of type III bursts (08:46–08:47 UT, not shown in the figure) preceded the type II burst, which appears at 08:48 UT and exhibits F-H structure. The starting frequency of the fundamental lane is 187 MHz and has a relative frequency drift rate of 0.011 s^{-1} .

The fourth event (August 9 2011, SOL2011-08-09T 07:48:00) was associated with an X6.9 class flare from AR

11263 (N17 $^{\circ}$ W69 $^{\circ}$), starting at 07:48 UT (08:05 peak) and a fast (1610 km/s) CME recorded by SoHO/LASCO at 08:12 UT with extrapolated lift-off at 07:52 UT. On the dynamic spectrum (Fig. 4) we have a group of type III bursts before the type II (F-H) and another III/U burst group starting near the onset time and frequency of the type II. The latter has a relative drift rate of 0.005 s^{-1} .

4. Fine structure

Fig. 5 shows a 15 s time interval of the first event (box in Fig.1) with 10 ms time resolution, which includes the shock front of the type II harmonic emission. In this and other events, the fundamental emission lane was outside of the SAO frequency range. In

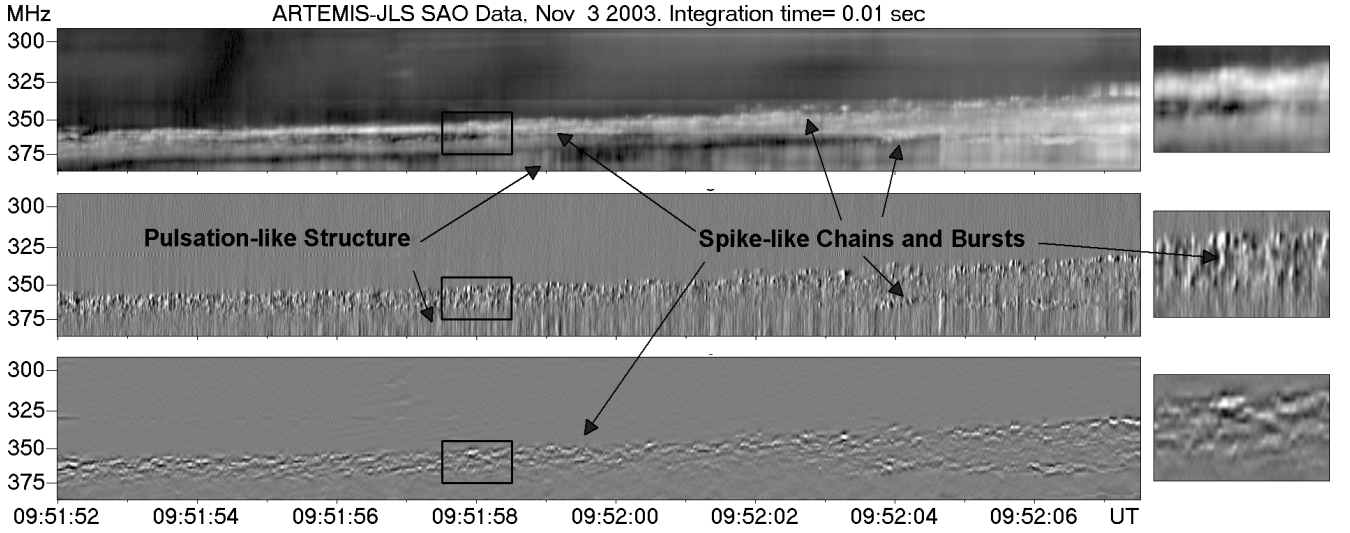


Fig. 5. Part of the high time resolution dynamic spectrum for the first event. The top panel shows the original spectrum, the middle panel the derivative with respect to time (differential spectrum), and the lower panel the spectrum after high pass filtering in time and frequency. The boxes indicate a 1 s by 30 MHz segment of the spectrum that is shown enlarged on the right. The arrows point at type II associated fine structures.

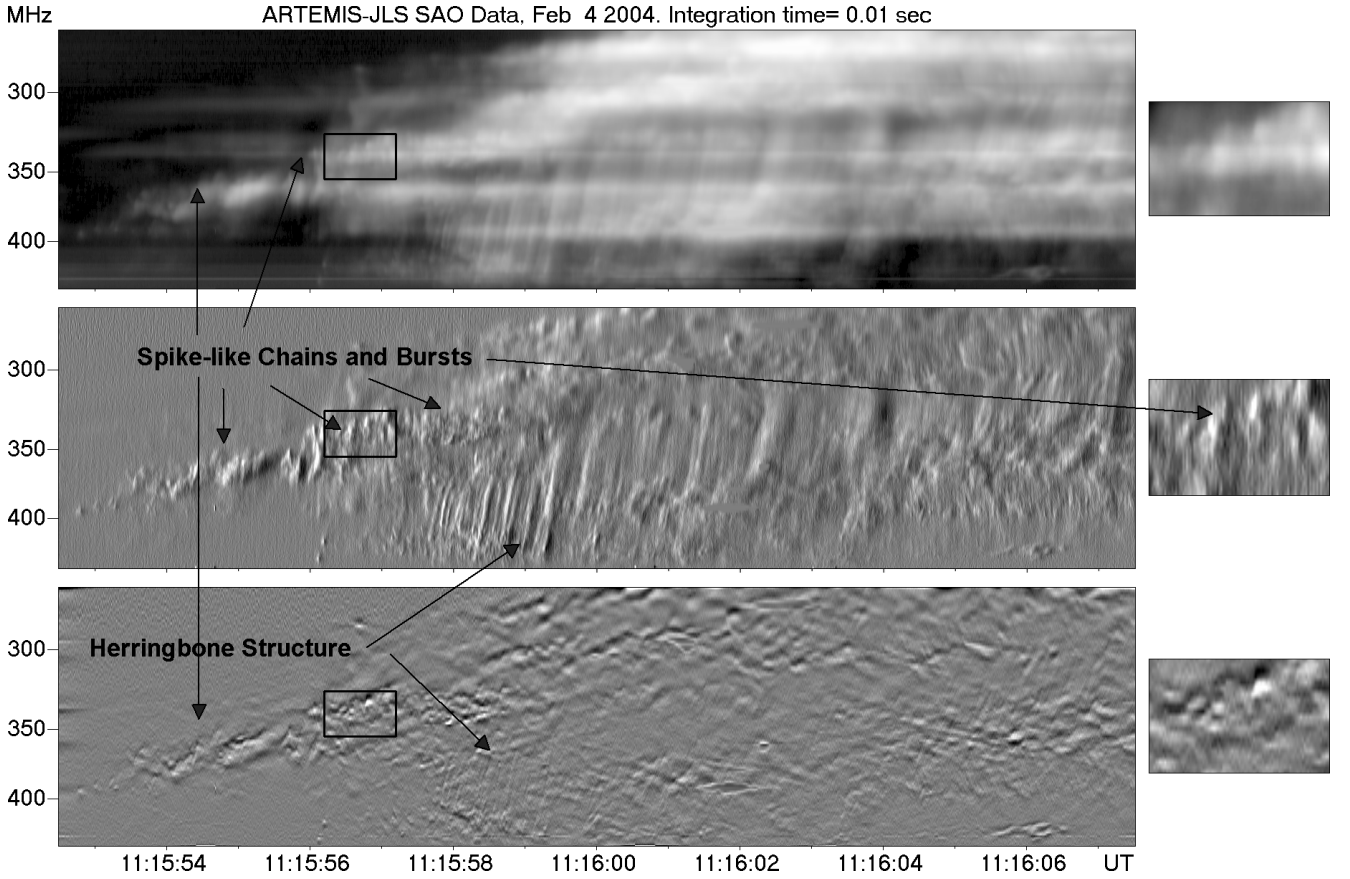


Fig. 6. Same as Fig. 5 for the second event.

addition to the original spectrum, we give its derivative with respect to time (differential spectrum) that enhances the fine structure and is less sensitive to receiver gain variations and radio interference signals. We also give the spectrum after the application of a high pass Gaussian filter with a width of 0.6 s by 5 MHz that suppressed large-scale structure; cf. Bouratzis et al. (2016).

We note a wealth of fine structure. The most prominent are chains of dot-like features resembling spikes commonly seen in type IV bursts. These chains are best visible in the filtered spectrum and are embedded in emission lanes, which drift almost parallel to one another and probably correspond to different regions of the expanding shock. In addition, we see high-drift structures before and during the chains, which are best visible in

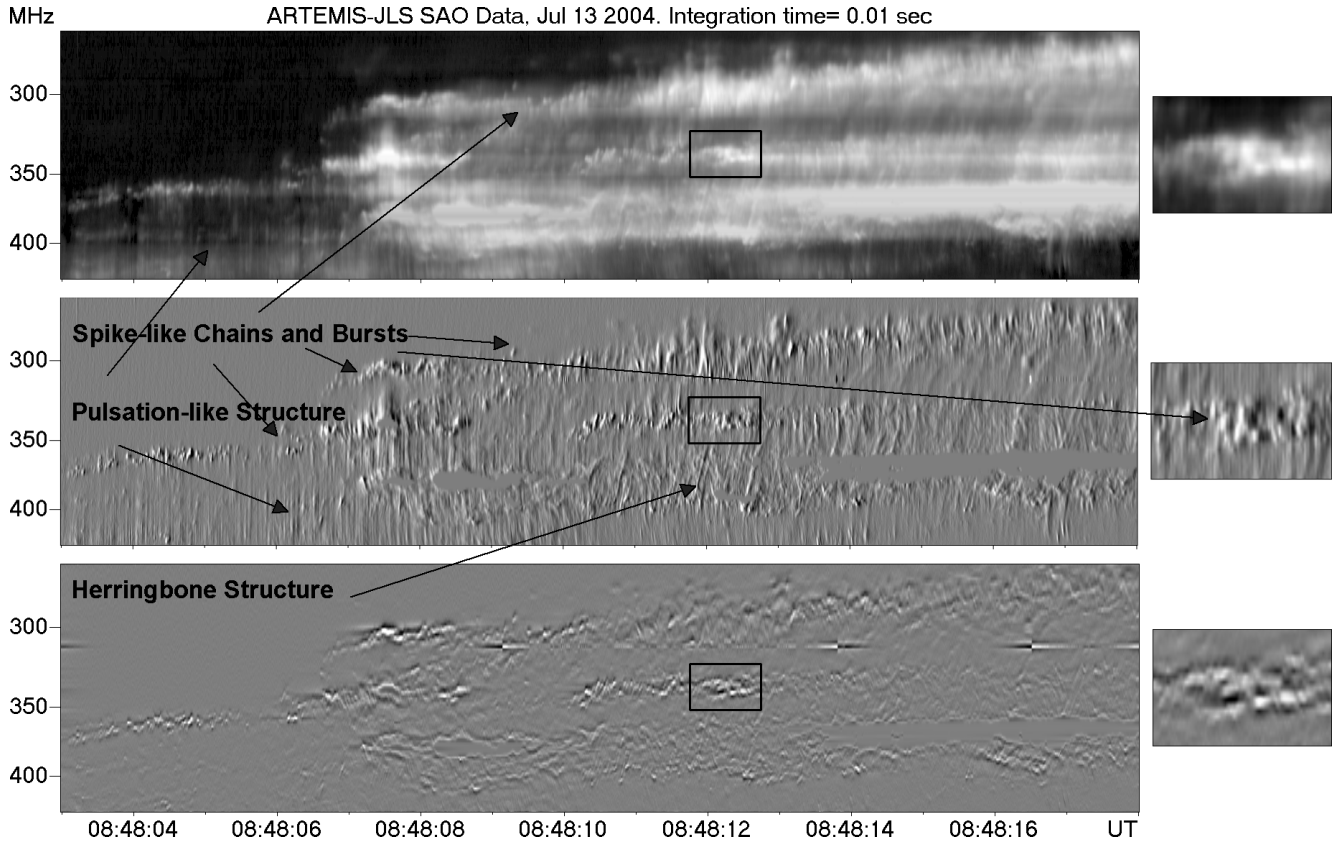


Fig. 7. Same as Fig. 5 for the third event. The uniform gray patches in the middle of the differential spectrum are due to saturation effects. Artifacts near 312 MHz in the filtered spectrum are due to interference signals.

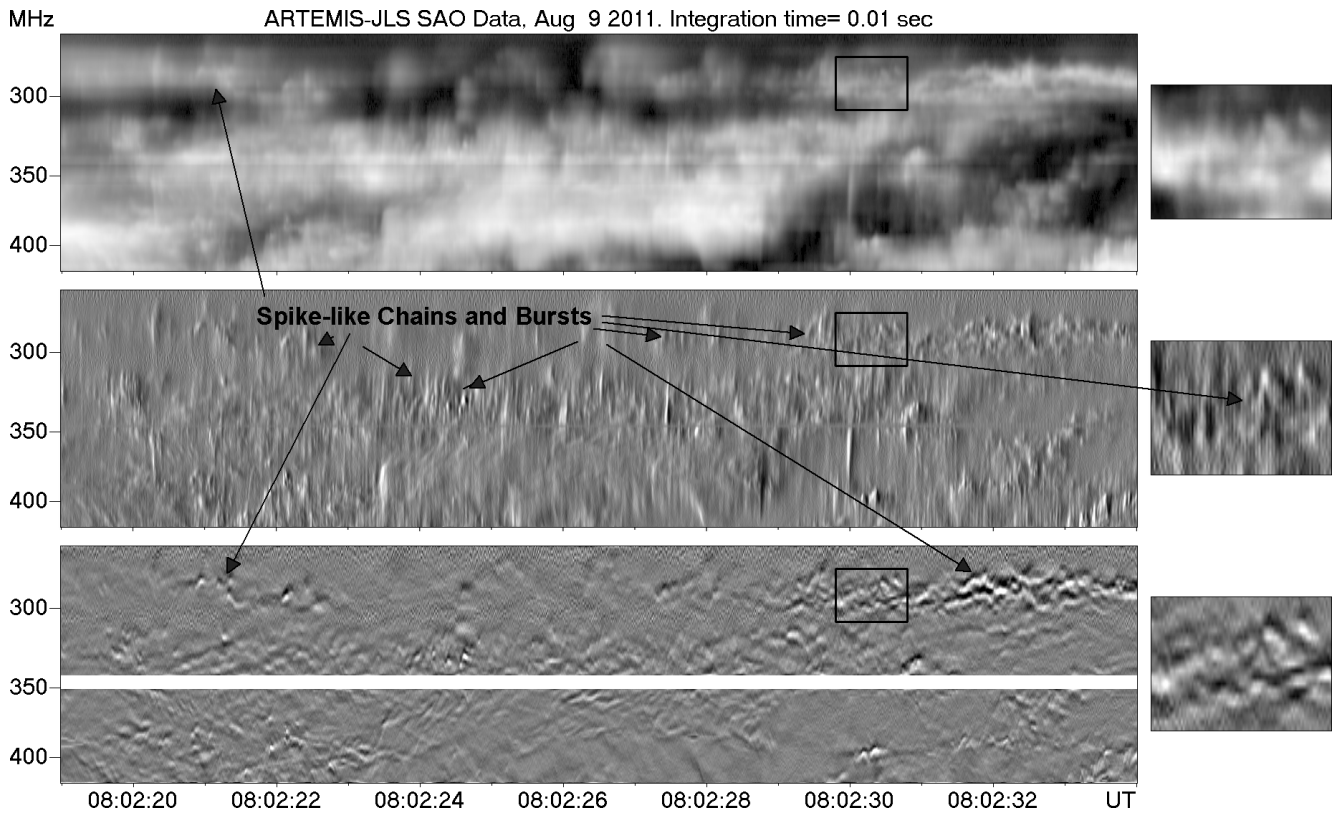


Fig. 8. Same as Fig. 5 for the fourth event. Some frequency channels around 350 MHz were strongly affected by radio interference and have been deleted in the filtered spectrum.

Table 1. Parameters of type II-associated spike-like bursts and type IV-associated spikes from Bouratzis et al. (2016).

Parameter	Type II spike-like bursts	Type IV spikes
Number of events	642	11579
Duration (ms)		
Average	96	100
Standard deviation	54	66
Relative bandwidth		
Average	1.7%	2.0%
Standard deviation	0.5%	1.1%

the differential spectrum. They are nearly vertical in the dynamic spectrum, hence they look more like pulsations rather than herringbones. These pulsation-like structures appear at frequencies higher than the type II lanes, drifting toward lower frequencies and seem to terminate at the spike chains.

In Fig. 6, we give a 15 s segment of the second event fine structure. This structure contains herringbones, chains of spike-like structures, and narrowband bursts of the type III family, and some of these appear in the gap between the two emission lanes. We note that a spike chain starts ~ 3 s before the main type II. The herringbones have a relative frequency drift rate of 0.55s^{-1} (speed ≈ 0.25 c under the assumption of four-fold Newkirk (1961) coronal density-height variation). The herringbone speed is consistent with published results by Cairns & Robinson (1987), Mann & Klassen (2005), and Carley et al. (2015).

The fine structure is similar in the third event, of which a 15 s dynamic spectrum is shown in Fig. 7. In this case the harmonic of the type II is almost entirely within the SAO frequency range and spike-like structures as well as herringbones were also recorded at the low frequency side of the type II (H). In this case again we have a spike chain before the start of the main type II.

A 15 s segment of the dynamic spectrum of the fourth event is given in Fig. 8. There are narrowband, spike-like structures in drifting chains during the shock and a more diffuse group at the onset of the Type II.

On the 10 ms SAO dynamic spectra we measured the instantaneous relative bandwidth ($\delta f/f$) and the total duration ($\delta\tau$) of 642 narrowband bursts. The identification of individual bursts was done by visual inspection, and the bandwidth and duration were measured after fitting the temporal and spectral profiles with a smooth curve as in Bouratzis et al. (2016, Fig. 3). In Table 1 we summarize the average parameters of the type II-associated spike-like structures. These parameters are very close to the corresponding parameters of type IV-associated spikes from Bouratzis et al. (2016, their Table 1), which are also included in the table for comparison.

The duration–frequency and bandwidth–frequency dependence of the spikes (narrowband structures) are usually expressed by phenomenological power laws of the form $\delta\tau \propto f^{-a}$, ($a \approx 1.32$) (Guedel & Benz 1990; Rozhansky et al. 2008; Sirenko & Fleishman 2009), and $\delta f \propto 0.66f^{0.42}$ by (Csillaghy & Benz 1993), respectively (see plots in Fig. 6 of Bouratzis et al., 2016). The present measurements are consistent with these empirical relations.

5. Summary and discussion

We observed a large number of spikes in metric type II radio bursts, using the SAO receiver of the Artemis-JLS radio spectro-

graph in the frequency range of 450–270 MHz. Their detection and the measurement of their duration and bandwidth was made possible thanks to the high sensitivity and time resolution of the instrument. As mentioned in the Introduction, Chernov (2016) reported fine structure, including spike-like structures, in a single decametric type II event. The author did not, however, elaborate further or provide any parameters of the observed structures to judge if these are similar to the spikes reported in this work.

Our comparison of the duration and bandwidth of type II associated spikes with those of type IV spikes (Table 1) show that they are very similar. The duration is comparable, while the difference in bandwidth is probably justified by the fact that its measurement depends both on the radio source size and the ambient density gradient, which is expected to vary considerably between disturbed plasma of the shock front and the type IV environment.

The vast majority of the spikes detected were aligned in chains along the type II lanes. The presence of spike-like fine structure in or near the type II lanes is probably a signature of non-thermal electrons originating in small-scale acceleration episodes. A possible candidate is an ensemble of reconnection events between the magnetic field downstream of the shock and the ambient magnetic field or preexisting magnetic structures.

In the future we expect to combine our spectral observations with imaging observations from the Nançay Radio Heliograph (NRH) to check the position of spikes with respect to that of the type II lanes. We will also examine our type II collection observed with the 100 ms resolution ASG receiver of Artemis-JLS for traces of spike structures in an effort to expand our sample of events.

Acknowledgements. The authors thank C. Karaberis for his assistance with the data reduction of the Artemis-IV/JLS observations. We also wish to thank the Onassis Foundation for financial support (Grant 15153) for the continued operation of the ARTEMIS-JLS radio spectrograph and the University of Athens Research Committee for Grant 15018. The anonymous reviewer provided useful suggestions, which have improved the quality of this article.

References

- Afanasyev, A. N. 2009, *Annales Geophysicae*, 27, 3933
 Bouratzis, C., Hillaris, A., Alissandrakis, C. E., et al. 2016, *A&A*, 586, A29
 Brueckner, G. E., Howard, R. A., Koomen, M. J., et al. 1995, *Sol. Phys.*, 162, 357
 Cairns, I. H. & Robinson, R. D. 1987, *Sol. Phys.*, 111, 365
 Carley, E. P., Reid, H., Vilmer, N., & Gallagher, P. T. 2015, *A&A*, 581, A100
 Caroubalos, C., Maroulis, D., Patavalis, N., et al. 2001, *Experimental Astronomy*, 11, 23
 Chernov, G. 2016, *Solar Flares: Investigations and Selected Research* (Nova Science Publishers, Inc.), ISBN: 978-1-53610-204-8
 Chernov, G. P. 1997, *Astronomy Letters*, 23, 827
 Chernov, G. P., Stanislavsky, A. A., Konovalenko, A. A., et al. 2007, *Astronomy Letters*, 33, 192
 Csillaghy, A. & Benz, A. O. 1993, *A&A*, 274, 487
 Gopalswamy, N., Yashiro, S., Michalek, G., et al. 2009, *Earth Moon and Planets*, 104, 295
 Guedel, M. & Benz, A. O. 1990, *A&A*, 231, 202
 Klassen, A., Pohjolainen, S., & Klein, K.-L. 2003, *Sol. Phys.*, 218, 197
 Kontogeorgos, A., Tsitsipis, P., Caroubalos, C., et al. 2006, *Experimental Astronomy*, 21, 41
 Krueger, A. 1979, *Geophysics and Astrophysics Monographs*, 16
 Mann, G. & Klassen, A. 2005, *A&A*, 441, 319
 Maxwell, A. & Thompson, A. R. 1962, *ApJ*, 135, 138
 Newkirk, G. J. 1961, *ApJ*, 133, 983
 Nindos, A. & Aurass, H. 2007, in *Lecture Notes in Physics*, Vol. 725, *The High Energy Solar Corona: Waves, Eruptions, Particles*, Berlin Springer Verlag, ed. K.-L. Klein & A. L. MacKinnon, 251–277
 Pick, M. & Vilmer, N. 2008, *A&A Rev.*, 16, 1
 Roberts, J. A. 1959, *Australian Journal of Physics*, 12, 327
 Rozhansky, I. V., Fleishman, G. D., & Huang, G.-L. 2008, *ApJ*, 681, 1688
 Sirenko, E. A. & Fleishman, G. D. 2009, *Astronomy Reports*, 53, 369
 Smerd, S. F., Sheridan, K. V., & Stewart, R. T. 1975, *Astrophys. Lett.*, 16, 23
 Vršnak, B. & Cliver, E. W. 2008, *Sol. Phys.*, 253, 215
 Vršnak, B., Magdalenic, J., & Zlobec, P. 2004, *A&A*, 413, 753